LBL-22258

EMITTANCE GROWTH IN INTENSE MISMATCHED BEAMS

O. A. Anderson and L. Soroka
Lawrence Berkeley Laboratory, University of California, Berkeley, CA 94720

We use analysis and numerical simulation to study transverse rms emittance growth in a space-charge dominated beam, mismatched to its transport channel. We discuss two cases: (I) a uniform cold beam injected into a slightly nonlinear channel, and (II) a semi-Gaussian beam injected into a linear channel. Nonlinear coupling damps the mismatch oscillations, converting the mismatch electrostatic energy into emittance growth. In case I, analysis shows a slow growth rate proportional to the channel nonlinearity parameter and predicts nearly complete damping and conversion to emittance growth; our simulations confirm these predictions. In case II the simulations show that damping is arrested and conversion is incomplete. Sequences of density profiles clarify this effect. The phase of the profile oscillations changes, after a few plasma periods, in a way that inhibits the rms emittance growth. The growth is entirely due to a halo that includes only a small fraction of the beam, unlike the situation in case I.

In general, there is little practical difference between phenomena in sheet beams and round beams,[1,2] but the analysis is usually much simpler in the former case. Therefore, in the present report we restrict ourselves to sheet beams.

We use the standard beam model[1] and again simplify our equations by omitting relativistic factors. Ref. 1 discusses how the correction γ^{-3} may be applied when appropriate.

Case I: Mismatched Beam in Nonlinear Channel

For a beam density $n(x,z)$, the number of particles per square centimeter within half-width x is

$$N_X(x,z) = \int_0^X n(x_1,z)\,dx_1, \qquad (1)$$

and the total number per square centimeter N is found by extending the upper limit to include all of the beam. Defining the normalized line perveance $P = 4\pi Ne^2/mv^2$ and the transverse space-charge electric field $4\pi eN_X$, we have the space charge term in the equation of motion

$$x'' = PN_X(x,z)/N - k_0^2 x(1+\sigma x^2/q^2). \qquad (2)$$

The second expression on the right represents an external focusing force with a cubic nonlinearity parameter σ. If the linear part of the force is F_e, then the focusing constant k_0^2 is defined by the expression $F_e/mv^2 = -k_0^2 x$. In Eq. (2), we have also introduced the transverse scale length $q = P/k_0^2$.

In a cold beam, the flow is initially laminar and the space-charge term in Eq. (2) is constant. We show later that it usually remains constant during most of the emittance growth. Writing the initial position $x(0)$ as ξ and the initial beam edge as h, we have for each particle in an initially uniform beam the constant quantity χ:

$$N_X/N = \xi/h \equiv \chi \qquad (3)$$

with $0 \le \chi \le 1$. Inserting Eq. (3) in Eq. (2) and solving, we obtain[2], to first order in μ and σ,

$$x(\chi,z) = q\chi[1-\sigma\chi^2+(\mu+\sigma\chi^2)\cos kz]; \qquad (4a)$$

$$k = k_0(1+\tfrac{3}{2}\sigma\chi^2) \qquad (4b)$$

with the mismatch parameter $\mu \equiv (h/q) - 1$.

Mean square beam size. To lowest order in μ and in the nonlinearity parameter σ,

$$x^2/q^2 = \chi^2 - 2\sigma\chi^4 + 2(\mu\chi^2+\sigma\chi^4)\cos[(1+\tfrac{3}{2}\sigma\chi^2)k_0 z].$$

For laminar flow, we take averages as in Ref. 1:

$$\langle x^2\rangle = N^{-1}\int_0^\infty d\xi\, n(\xi)\, x^2(\xi,z), \qquad (5)$$

so

$$\langle x^2\rangle = \int_0^1 x^2(\chi)\,d\chi = q^2[1/3 - 2\sigma/5 + 2\mu I_1 + 2\sigma I_2],$$

where I_1 and I_2 are combinations of trigonometric functions and Fresnel integrals. We see the effect of the nonlinearity parameter σ by expanding this result for large z. We obtain the leading terms

$$\langle x^2\rangle = q^2\left[\frac{1}{3} - \frac{2\sigma}{5} + \frac{2}{3\sigma k_0 z}(\mu+\sigma)\sin k_0 z\right] \qquad (6)$$

The z^{-1} damping of the envelope oscillations implies transferrence of energy to emittance growth[2]. Eventually laminarity ceases and Eq. (6) loses accuracy, but, as we shall see, not necessarily before the emittance growth is essentially complete. Fig. 1a shows a simulation result which for large z agrees closely with Eq. (6).

Phase configuration. Eq. (4) gives, to lowest order,

$$x'(\chi,z) = -k_0 q\chi(\mu+\sigma\chi^2)(1+\tfrac{3}{2}\sigma\chi^2)\sin[(1+\tfrac{3}{2}\sigma\chi^2)k_0 z], \qquad (7)$$

which, with Eq. (4), gives the phase configuration. The beam edge oscillates at different frequency from the center; the growing irregularity causes rms emittance growth, as illustrated in Fig. 1b.

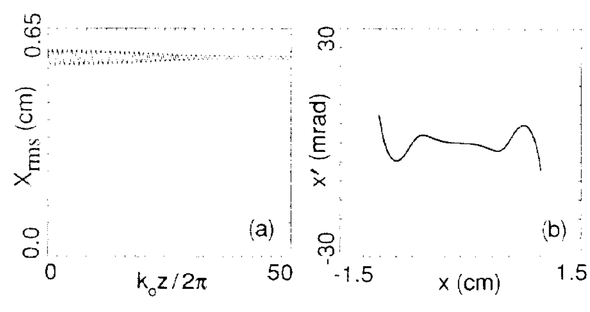

Fig. 1. (a) Damping of envelope oscillations for $\mu = 0.03$, $\sigma = 0.02$. (b) Phase-space configuration at $k_0 z/2\pi = 40$.

Rms Emittance. As in Ref. 2, we use Sacherer's definition of mean square emittance,

$$\epsilon^2 = \langle x^2\rangle\langle x'^2\rangle - \langle xx'\rangle^2 \qquad (8)$$

We evaluate $\langle x'^2\rangle$ and $\langle xx'\rangle$ in terms of Fresnel integrals and expand these for small and large z.

Small z. To lowest order in μ and σ, the mean growth rate is[2]

$$\epsilon^2 = \frac{P^4}{6\cdot 7\cdot 25\, k_0^6}[4\sigma^2 + A_1\zeta^2 - \cdots], \qquad (9a)$$

$$A_1 = (\mu^2 + \tfrac{10}{9}\mu\sigma + \tfrac{5}{21}\sigma^2). \qquad (9b)$$

We have defined the normalized distance $\zeta = 3\sigma k_0 z$ and have omitted all oscillatory terms, as discussed in Ref. 2. During the main part of the emittance growth, the A_1 term dominates and the growth rate is

$$\frac{d\epsilon}{dz} \cong \left[\frac{3A_1}{2\cdot 175}\right]^{1/2}\frac{\sigma P^2}{k_0^2}. \qquad (10)$$

CH2387-9/87/0000-1043 $1.00 © IEEE

Large z. To lowest order in ζ^{-1}, again omitting oscillatory terms,

$$\epsilon(\zeta) = \frac{p^2}{k_0^3\sqrt{18}}\left[\left(\mu^2 + \frac{6}{5}\mu\sigma + \frac{3}{7}\sigma^2\right) - \frac{9}{\zeta^2}(\mu+\sigma)^2\right]^{1/2}. \quad (11)$$

To get the asymptotic value ϵ_∞ we neglect the last term. Typically, $\sigma \lesssim \mu$, so that $\epsilon_\infty \propto \mu$, i.e., the final emittance is proportional to the mismatch, as might be expected.

We divide ϵ_∞ by Eq. (10) to find the nominal growth distance

$$k_0 z_{growth} = \frac{\sqrt{175}}{3^{3/2}\sigma}\left[1 + \frac{2}{45}\frac{\sigma}{\mu} + \cdots\right]. \quad (12)$$

In the typical case $\sigma \lesssim \mu$, we see that $z_{growth} \propto 1/\sigma$. The growth rate is proportional to the nonlinearity parameter.

Laminarity. The flow is laminar up to the critical distance given by[2] $3\sigma k_0 z_{crit} \cong (\mu+\sigma)^{-1}$, so that the condition for growth to be essentially complete during laminar flow is

$$\mu + \sigma < (3/175)^{1/2}. \quad (13)$$

Analysis vs. Simulation. Equations (9) and (11) describe the growth of emittance to lowest order in the mismatch and nonlinearity parameters. Fig. 2a shows the result for the case $\mu = 0.03$, $\sigma = 0.02$, for which the laminarity criterion, Eq. (13), is well satisfied. The simulation for this case, Fig. 2b, shows the exact solution, including the oscillations which we chose to suppress in the analysis.

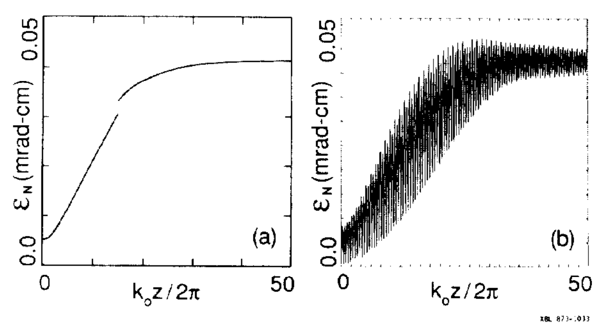

Fig. 2. Emittance growth from mismatch in nonlinear channel. (a) Small z [Eq. (9)] and large z [Eq. (11)] analytic results. (b) Simulation result.

Case II: Mismatched Beam in a Linear Channel

It is not easy to get analytic results for this case because the entire effect depends on non-laminar flow. However, one can appeal to conservation of energy and note that there is a large electrostatic energy associated with beam mismatch, so that the emittance growth could be large. (Formulas are derived in Ref. 2.) The energy argument does not determine how much of this electrostatic energy is eventually converted to rms emittance (disordered motion) and how much simply persists as a coherent oscillation.

Some insight is obtained from what is known as Wangler's equation.[3-6] The sheet-beam version is[1]

$$\frac{d}{dz}\epsilon^2 = -\frac{p}{\sqrt{3}} X^3 \frac{d}{dz} U_n, \quad (14)$$

where $X = \langle x^2\rangle^{1/2}$ and where U_n is the normalized free energy or shape factor[1], which is zero for a uniform beam. We assume that the mismatched beam size X oscillates nearly sinusoidally over a given period. Then, if the oscillation period is $2\pi/k_1$, we have

$$X \cong \bar{X} + \delta X \cos k_1 z,$$
$$X^3 \cong \bar{X}^3 + 3\,\delta X\,\bar{X}^2 \cos k_1 z + O(\delta X^2). \quad (15)$$

The overbars indicate an average over the given period. The U_n oscillations usually have pronounced harmonic content, so we write

$$U_n = \bar{U}_n + \delta U_n \cos(k_1 z + \phi) + \text{harmonics},$$
$$U_n'(z) = -k_1\,\delta U_n \sin(k_1 z + \phi) + \text{harmonics}, \quad (16)$$

with a phase difference ϕ with respect to X. We multiply Eq. (15) by (16) and integrate over the given period. If we drop the $O(\delta X^2)$ terms, the harmonics do not contribute, and the growth during the period, from Eq. (14), is

$$\Delta\epsilon^2 = \frac{\sqrt{3}}{2} p\, \bar{X}^2\, \delta X\, \delta U_n \sin\phi. \quad (17)$$

If the profile oscillations lag significantly behind the envelope oscillations, there will be emittance growth proportional to the variations in X and in U_n. But if eventually the shape and size vary together, the growth stops.

Simulation for Semi-Gaussian Case. Figure 3 shows numerical simulations for $X(z)$, $U_n(z)$, and $\epsilon^2(z)$ which confirm Eq. (17). Near the beginning (Fig. 3a) the profile oscillations lag behind (by nearly 90^0) giving maximum growth rate for ϵ. Further on (Fig. 3b), the oscillations become synchronized and the growth stops.

Fig. 4a shows phase plots and density profiles for a semi-Gaussian initial configuration, the same case used for Fig. 3. One sees two corners of the distribution function rotating in phase space faster than the core so that a halo develops. The density profiles show that this halo contains only a small fraction of the beam. These

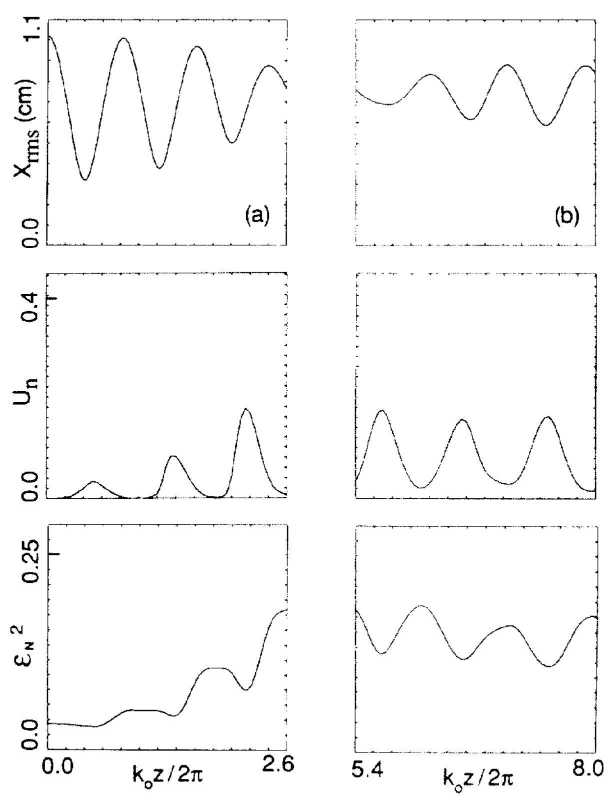

Fig. 3. (a) Emittance growth during period when U_n lags X. (b) Stationary emittance after U_n pulsates with X.

profiles are displayed at z values that coincide with the minima and maxima of the shape factor U_n in Fig. 3.

Fig. 4b illustrates the synchronized regular breathing of the beam size and shape which occurs later (cf. Fig. 3b). The halo accounts for all the emittance growth; if a small percentage of the beam were eliminated, the rms emittance would be no greater than the original value. This illustrates a general principal: rms results can be quite misleading for functions with long tails.

In comparison, a weakly nonlinear channel (Part I) gives slower emittance growth, but the final effect may be more significant because all of the beam is involved, not just a halo.

Acknowledgments

We wish to thank LLoyd Smith, Chris Celata, Denis Keefe, and other members of the LBL HIF group for valuable discussions. This work was supported by US DOE Contract DE-AC03-76SF00098.

References

1. O.A. Anderson, Lawrence Berkeley Laboratory report LBL-19996; to be published in Particle Accel. An abridged version was published in the Proceedings of the 1986 Linear Accelerator Conference, Stanford Linear Accelerator Center, June 2-6, 1986, SLAC Report 303, p. 65.
2. O.A. Anderson, International Symposium on Heavy Ion Fusion, Washington, D.C., May 27-29, 1986, AIP Conference Proc. No. 152, p. 253.
3. P.M. Lapostolle, CERN-ISR-DI/71-6 (1971). P.M. Lapostolle, IEEE Trans. Nucl. Sci., 18, 1101 (1971).
4. E.P. Lee, S.S. Yu, and W.A. Barletta, Nuclear Fusion, 21, 961 (1981).
5. J. Struckmeier, J. Klabunde, and M. Reiser, Particle Accel., 15, 47 (1984).
6. T.P. Wangler, K.R. Crandall, R.S. Mills, and M. Reiser, IEEE Trans. Nucl. Sci., 32, 2196 (1985).

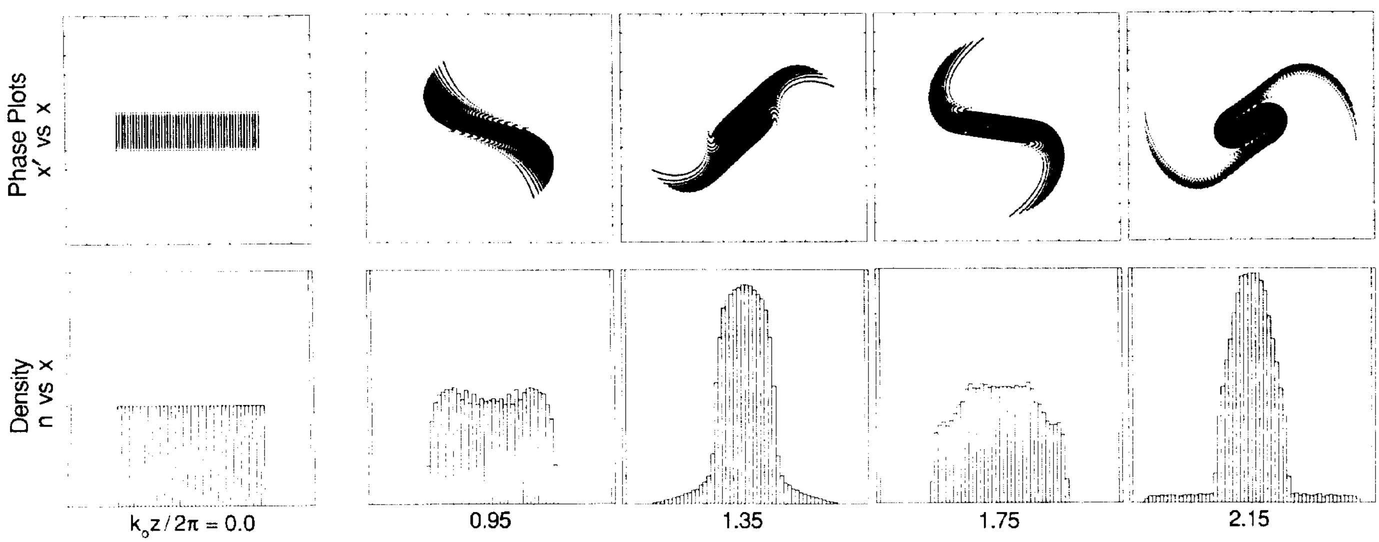

Fig. 4a. Phase plots and density profiles during the period of rms emittance growth. The initial distribution is a truncated semi-Gaussian. As in Fig. 3, the initial tune depression (ω/ω_0) is 0.26 and the mismatch is 44%.

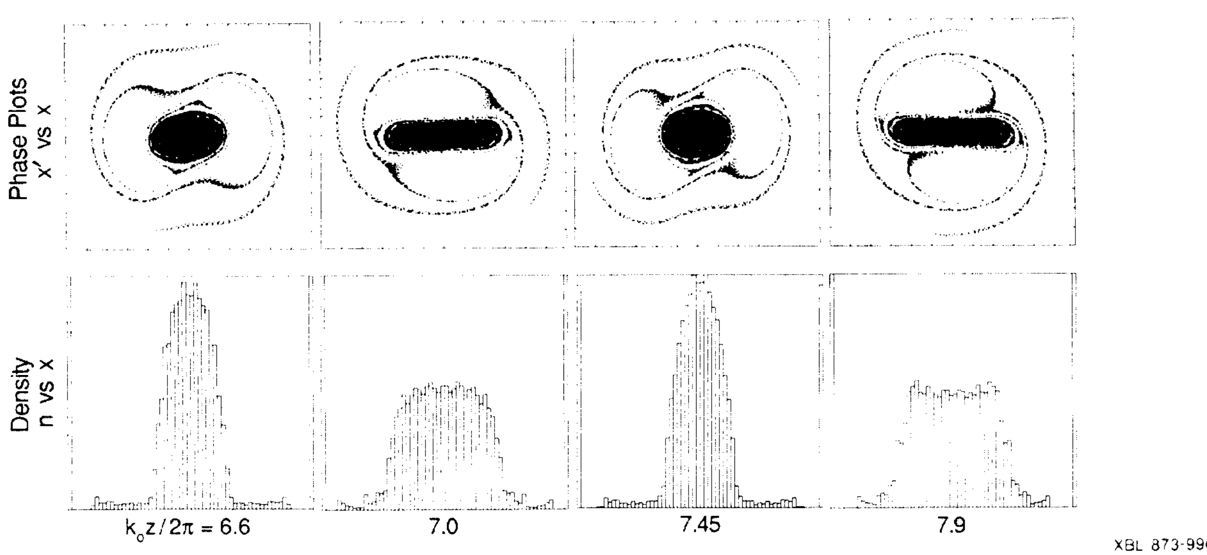

Fig. 4b. The same case after saturation of the rms emittance.